

# Bidirectional reflectance and polarization measurements on packed surfaces of benthic sediments and spherical particles

Hao Zhang<sup>1,2,\*</sup> and Kenneth J. Voss<sup>1</sup>

<sup>1</sup>Department of Physics, University of Miami, Miami, FL 33124, USA

<sup>2</sup>Current address: NOAA/NESDIS/STAR, 5200 Auth Road, Room 102, Camp Springs, MD 20746, and CIRA, Colorado State University, Fort Collins, CO, USA

\*Corresponding author: [Hao.Zhang@NOAA.GOV](mailto:Hao.Zhang@NOAA.GOV)

**Abstract:** Laboratory bidirectional reflectance and polarization measurements were carried out on packed layers of both natural sediments and manufactured spherical particles. The results indicate that among the natural sediments showing a strong backscattering peak (“hotspot”), the rough platelets are the only sediments with a branch of negative polarization. Measurements of circular and linear polarization ratios indicate that both smooth ooids and rough platelets are strongly depolarizing. Measurements of perfect spherical grains show both negative polarization and strong backscattering as a remnant of the single scattering process.

©2009 Optical Society of America

**OCIS codes:** 010.4450 Ocean optics, 030.5620, Radiative transfer, 120.5820 Scattering measurements, 240.6490 Spectroscopy, surface 290.1483 BSDF, BRDF, BTDF, 290.4210 Multiple scattering.

---

## References and links

1. B. Hapke, *Theory of reflectance and emittance spectroscopy* (Cambridge Univ., 1993).
2. K. Muinonen, “Coherent backscattering by solar system dust particles,” *Asteroids, Comets, Meteors* **160**, 271-296 (1993).
3. Y. G. Shkuratov, K. Muinonen, E. Bowell et al. “A critical review of theoretical models of negatively polarized light scattered by atmosphereless solar system bodies,” *Earth, Moon and Planets* **65**, 201-246 (1994).
4. M. I. Mishchenko, L. D. Travis, and A. A. Lacis, *Multiple Scattering of Light by Particles: Radiative Transfer and Coherent Backscattering* (Cambridge Univ., 2006).
5. M. I. Mishchenko, “On the nature of the polarization opposition effect exhibited by Saturn’s rings,” *Astrophys. J.* **411**, 351-361 (1993).
6. M. I. Mishchenko, V. K. Rosenbush, and N. N. Kiselev, “Weak localization of electromagnetic waves and opposition phenomena exhibited by high-albedo atmosphereless solar system objects,” *Appl. Opt.* **45**, 4459-4463 (2006).
7. P. M. Saulnier, M. P. Zinkin, and G. H. Watson, “Scatterer correlation effects on photon transport in dense random media,” *Phys. Rev. B* **42**, 2621-2623 (1990).
8. B. W. Hapke, R. M. Nelson, and W. D. Smythe, “The opposition effect of the moon: the contribution of coherent backscatter,” *Science* **260**, 5107-5109 (1993).
9. Y. G. Shkuratov, M. A. Kreslavsky, A. A. Ovcharenko, D. G. Stankevich, and E. S. Zubko, “Opposition effect from Clementine data and mechanisms of backscatter,” *Icarus* **141**, 132-155 (1999).
10. Y. Shkuratov, A. Ovcharenko, E. Azubko, O. Miloslavskaya, K. Muinonen, J. Piironen, R. Nelson, W. Smythe, V. Rosenbush, and P. Helfenstein, “The opposition effect and negative polarization of structural analogs for planetary regoliths,” *Icarus* **159**, 396-416 (2002).
11. M. I. Mishchenko, J. M. Luck, and T. M. Nieuwenhuijzen, “Full angular profile of the coherent polarization opposition effect,” *J. Opt. Soc. Am.* **A17**, 888-891 (2000).
12. M. I. Mishchenko, “The angular width of the coherent back-scatter opposition effect: an application to icy outer planet satellites,” *Astrophys. Space Sci.* **194**, 327-333 (1992).
13. B. Hapke, D. DiMucci, R. Nelson, and W. Smythe, “The cause of the hot spot in vegetation canopies and soils: shadow hiding versus coherent backscattering,” *Remote Sens. Environ.* **53**, 63-68 (1996).
14. B. Hapke, R. Nelson, and W. Smythe, “The opposition effect of the moon: Coherent backscatter and shadow hiding,” *Icarus* **133**, 89-97 (1998).

15. G. D. Gilbert and J. C. Pernicka, "Improvement of underwater visibility by reduction of backscatter with a circular polarization technique," *Appl. Opt.* **6**, 741-746 (1967).
16. G. D. Lewis, D. L. Jordan, and P. J. Roberts, "Backscattering target detection in a turbid medium by polarization discrimination," *Appl. Opt.* **38**, 3937 – 3944 (1999).
17. K. J. Voss and E. S. Fry, "Measurement of the Mueller matrix for ocean water," *Applied Opt.* **23**, 4427-4439 (1984).
18. H. Zhang and K. J. Voss, "Comparisons of bidirectional reflectance distribution function measurements on prepared particulate surfaces and radiative-transfer models," *Appl. Opt.* **44**, 597-610 (2005).
19. H. Zhang and K. J. Voss, "Bi-directional reflectance measurements of closely packed natural and prepared particulate surfaces," in *Light Scattering Reviews 3*, A. A. Kokhanovsky ed. (Springer-Praxis, 2008).
20. H. Zhang, K. J. Voss, R. P. Reid, and E. M. Louchard, "Bidirectional reflectance measurements of sediments in the vicinity of Lee Stocking Island, Bahamas," *Limnol. Oceanogr.* **48**, 380-389 (2003).
21. H. Zhang and K. J. Voss, "Bi-directional reflectance study on dry, wet and submerged particulate surfaces," *Appl. Opt.* **45**, 8753-8763 (2006).
22. Y. Shkuratov and Y. S. Grynko, "Light scattering by media composed of semitransparent particles of different shapes in ray optics approximation: consequences for spectroscopy, photometry and polarimetry of planetary regoliths," *Icarus* **173**, 16-28 (2005).
23. S. Bondarenko, A. Ovcharenko, Y. Shkuratov, G. Videen, J. Eversole, and M. Hart, "Light backscatter by surfaces composed of small spherical particles," *Appl. Opt.* **45**, 3871-3877 (2006).
24. K. J. Voss and H. Zhang, "Bidirectional reflectance of dry and submerged Labsphere Spectralon plaque," *Appl. Opt.* **45**, 7924-7927 (2006).
25. C. Bruegge, N. Chrien, and D. Haner, "Spectralon BRDF data for MISR calibration applications," *Remote Sens. Environ.* **76**, 354-366 (2001).
26. M. I. Mishchenko, J. M. Dlugach, E. G. Yanovitskij, and N. T. Zakharova, "Bidirectional reflectance of flat, optically thick particulate layers: an efficient radiative transfer solution and applications to snow and soil surfaces," *J. Quant. Spectrosc. Radiat. Transfer* **63**, 409-432 (1999).
27. H. C. van de Hulst, *Light Scattering by Small Particles* (Dover, 1981).

## 1. Introduction

The brightness enhancement toward zero phase angle (angle between incident and reflected light) observed in light scattering by many media such as astronomical bodies and terrestrial surfaces is widely known as the "hot spot" or opposition effect [1]. Strictly speaking, the term opposition effect only refers to the nonlinear brightness surge toward the exact backscattering direction. However, for many surfaces the angular width of the hot spot peak is much wider (e.g., lunar regolith), and hence this term has often been used to describe the enhanced backscattering in a broader sense [2]. Moreover, it is found that the hotspot is often accompanied by a branch of negative polarization (BNP). Specifically, when unpolarized light is scattered by a rough surface, it may become partially linearly polarized [3]. The degree of polarization (DOP) is defined as:

$$DOP = \frac{I_{\perp} - I_{\parallel}}{I_{\perp} + I_{\parallel}}, \quad (1)$$

where  $I_{\perp}$  and  $I_{\parallel}$  are the scattered intensities polarized in directions normal and parallel to the scattering plane (the plane containing the incident and emergent directions), respectively. A BNP often manifests itself as a decreasing DOP from larger phase angles, reaching a minimum, negative, value at a small phase angle and increasing to 0 at  $0^{\circ}$  phase angle. The width of BNP is found to be about  $25^{\circ}$  for many particulate surfaces. In contrast, the DOP is always positive for Fresnel reflection and first-order Rayleigh scattering.

Classically the hotspot had been explained as the shadow hiding opposition effect (SHOE) since along the backscattering direction all particles would hide their own shadows [1]. The more recently proposed coherent backscattering (CBS) mechanism, which explains the narrow opposition surge as the interference between the incoming and outgoing rays in the same optical path, has been used extensively to interpret photometric curves at small phase angles in recent years [Ref. 4 and references therein]. A CBS typically manifests two prominent features: (1) a narrow nonlinear intensity peak centered at opposition superimposed on a linear

background, and (2) a sharp and narrow asymmetric negative polarization peak with an angular width (typically less than  $2^\circ$ ) commensurate with the intensity opposition peak (the polarization opposition effect, see, e.g., Refs.[5,6]).

An approximate scalar theory of CBS has proposed that the surge has a full angular width (in radians) on the order of

$$\Delta g \approx \frac{0.72}{kl^*}, \quad (2)$$

where  $k = \frac{2\pi}{\lambda}$  with  $\lambda$  the wavelength of the incident radiation,  $l^*$  is the so-called photon transport mean free path given by [7]

$$l^* = \frac{1}{n\sigma Q_{sca}(1 - \langle \cos \theta \rangle)}, \quad (3)$$

where  $n$  is the number density of the particles,  $\sigma$  the average particle geometric cross section,  $Q_{sca}$  the scattering efficiency and  $\langle \cos \theta \rangle$  the asymmetry parameter of the particle scattering phase function. According to Eqs. (2) and (3), if the particle size is taken as the quantity  $l^*$ , particles much larger than the radiation wavelength would exhibit a very narrow CBS peak. For example, for micrometer-sized grains  $\Delta g \sim 2^\circ$  while for millimeter-sized grains this value decreases to about  $0.002^\circ$ . However, in planetology it has been speculated that the CBS may characterize micrometer-sized surface asperities in lunar regolith grains and thus the CBS could extend to larger phase angles [8]. Suggestions have also been made that the CBS may extend to  $10^\circ$  in micrometer-sized grain layers with moderate albedo [9,10]. Note that rigorously, the angular width of CBS may also depend on the polarization state of the incident radiation [11] and a dense-medium light scattering theory shows that the angular width of the CBS is limited to  $2^\circ$  or so [6,12].

While it is widely observed that many particulate layers, especially those composed of micrometer-sized grains and smaller, may have a narrowly peaked CBS peak superimposed on a wider SHOE background, at present there seems to be few widely accepted quantitative methods to distinguish CBS from SHOE. One proposed empirical approach is to look at the circular polarization ratio (CPR) [8,13,14]. The CPR ( $\mu_c = I_{CS}/I_{CO}$ ) defined as the ratio of the scattered radiance with the same helicity as the incident light,  $I_{CS}$ , to that with the opposite helicity,  $I_{CO}$ . In going from large phase angle toward opposition, if  $\mu_c$  decreases monotonically, the enhanced backscattering is caused by SHOE; if  $\mu_c$  increases toward zero phase angle, the hotspot is likely caused by CBS. Measurements on returned lunar regolith samples with a typical grain size of  $40 \mu\text{m}$  indicate that  $\mu_c$  starts to increase below  $6^\circ$  phase angle at 633 nm illumination [8]. This approach is based on the following argument. Specular reflection by a particle's surface constitutes a large contribution to backscattering and Fresnel reflection always reverses the helicity of circularly polarized incident light. In contrast multiple scattering by a rough surface would randomize the incident polarization. Since the nature of shadow hiding is single scattering while the CBS is multiple scattering, toward opposition it is expected that the reflected light would have a monotonically decreasing  $\mu_c$  for SHOE but an increased  $\mu_c$  for CBS.

In addition, polarization, both linear and circular, has been seen as a way to enhance contrast in a scattering medium [15,16]. This method depends on the contrast in the polarized scattering between the medium and the target. Mueller matrix measurements of the water [17] show that scattering by water would cause  $\mu_c < 0.2$ . In-water applications of this technique depend on the difference between this and a target (sediment in this case) depolarizing light ( $\mu_c = 1$ ). For linear polarization, because of the geometry, there are actually two variations of

this parameter  $\mu_{\perp} = I_{SP} / I_{SS}$  and  $\mu_{\parallel} = I_{PS} / I_{PP}$  where  $\mu_{\perp}$  and  $\mu_{\parallel}$  are defined with incident light perpendicular (“S”) and parallel (“P”) to the scattering plane, respectively ( $I_{PS}$  is perpendicularly polarized scattered radiance with a parallel polarized incidence, and so forth). In this case, once again the Mueller matrix for water shows that  $\mu_{\perp} = \mu_{\parallel} = 0$ , while a depolarizing surface has  $\mu_{\perp} = \mu_{\parallel} = 1$ .

The samples used in the laboratory polarization measurements mentioned above are mostly fine lunar regolith and planetary surface analog materials having particle sizes of several or a few tens of micrometers. In our measurements of the bi-directional reflectance distribution function (BRDF) of both natural benthic sediments and prepared particulate layers [18,19], we have found significant hotspots in most of the millimeter-sized samples [20,21]. Although in underwater remote sensing it would be difficult to acquire scattering information within 2° phase angle (except in the case of lidar measurements), given the CBS and SHOE characterization efforts summarized above, we wanted to answer the following questions; is negative polarization observable in these millimeter-sized benthic sediment grains? Can we possibly detect any CBS features, or distinguish CBS from SHOE at > 2° phase angle, in sediment reflectance? To what extent do sediment particles depolarize the light? Also, since controlled laboratory measurements on spherical particles are helpful in understanding radiative transfer in packed layers [18,22,23], we investigated the polarization properties of backscattered light from packed spherical particles.

## 2. Instrument and measurement

The goniometer used in this work, shown in Fig. 1, is an improved version of the instrument described earlier [18] with modifications to improve the angular resolution and simplify polarization measurements [24]. In this system, light from a He-Ne laser (633 nm) is inserted into an Edmund multimode fiber through a focusing assembly. The multimode fiber is used to depolarize the laser light (and has been found to reduce DOP to less than 1%). After exiting the fiber, the light is collimated by a lens and illuminates a small region of the sample surface (7 mm diameter when incident normal to the surface). The viewing optics consists of a focusing lens, an interference filter at the laser wavelength, and a Hamamatsu S8745 silicone photodiode. These optics are configured to view a 7 cm diameter area on the surface. The distance between the viewing tube assembly stop (with an aperture diameter of 1.5 cm) and the sample surface is 111 cm which gives an angular resolution of 0.8° full angle. For both incident and viewing tube assemblies, a linear polarizer (Melles Griot 03FPG) and a quarter wave plate (CVI QWPM-633) can be added to select the desired polarization combinations. To increase signal-to-noise we chop the incident laser beam, and the received signal is processed by a Stanford Research SR 830 lock-in amplifier before it is digitized by a NIDAQ-700 PCMCIA card (National Instruments) in a laptop computer.

We normalize the radiance scattered by the sample to the radiance obtained with a 99% Lambertian plaque (Labsphere) and multiply this by the reflectance factor (REFF) [24] of the plaque to get the REFF of the sample. This allows an easy comparison to a perfect Lambertian surface. Measurements were done at normal, 8°- and 60°-incidence. These incident angles were selected because there are published data for the Labsphere plaque [25] so we can accurately calibrate the measured reflectance. In addition the 60° incident angle enables us to sample a larger range of phase angles. The minimum phase angle that can be achieved is about 1.5° while the largest would depend on the incident angle. Measurements were done in the principal plane, which is the plane including the incident and viewing directions. Typically data were recorded every 1-2° near opposition, every 2-5° in the forward direction, and every 0.5° in the rainbow regions (for spheres only).

The typical extinction ratios for the polarizers used were estimated by pointing the viewing tube assembly directly to the incident tube assembly and setting the polarizer to obtain the minimum transmission (“crossed”). For the two linear polarizers the extinction ratio was found to be 700. For the two sets of circular polarizers (linear polarizer + quarter wave plate),

the extinction ratio was approximately 350. These ratios include electronic noise due to the data acquisition systems.

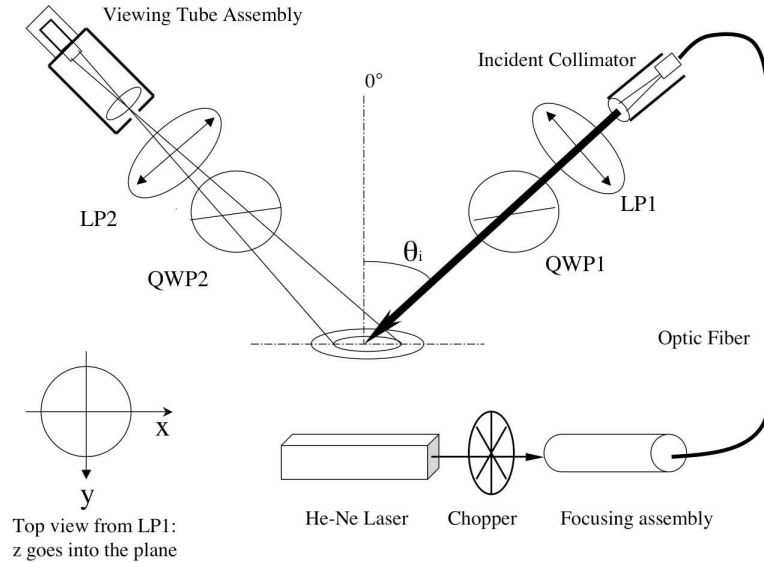


Fig. 1. Schematic of the polarized goniometric system. LP-linear polarizer; QWP-quarter wave plate. In reality, LP1 and QWP1 are inside the incident tube assembly and LP2 and QWP2 are inside the viewing tube assembly. The y axis is the normal of the scattering plane and the direction of perpendicular (“S”) linear polarization, and x is the parallel (“P”) direction.

Measurement uncertainty is estimated from repeated measurements on both the same surface and different surface realizations, and was found to vary significantly from surfaces with various brightness levels and grain sizes, and with different incident and viewing configurations. In general a lower uncertainty was found for (1) brighter samples due to their higher signal-to-noise ratio (SNR), (2) near-normal incident and viewing angles due to higher irradiance and higher collection efficiencies, and (3) samples with smaller grains due to relatively more sampled particles. However there are exceptions. For example, for non-absorbing spherical particles a radiometer with limited angular resolution may miss the sharp peak of a rainbow in one measurement and thus give apparently inconsistent repeated results in the rainbow regions. For measurements on randomly orientated large glass frits the glare at some angular positions produced by individual facets are almost impossible to reproduce in the next surface realization. For brighter samples measurement uncertainties are estimated to be 1-2% for normal REFF and 1-7% for  $60^\circ$ -incidence REFF; for dark volcanic sands, these values are at least doubled. Measurement uncertainty increases significantly for polarization measurements due to the much lower SNR. Repeated measurements on  $\mu_c$  demonstrate that for brighter samples the typical uncertainty is about 3-4% for most angle ranges but can exceed 20% for dark volcanic sand. By applying error propagation to Eq. (1), the measured DOP would have an uncertainty of several tens percent for the worst case, and this causes repeated DOP values to vary around zero for all samples except the bright spheres. For this reason we look at the general trend of the measured DOP curves instead of values at some specific points, and rely on repeated measurements for detection of the BNP.

### 3. Results and discussions

We chose four typical samples from our collection of natural sediments and manufactured spheres. The first natural sediment is composed of 1–2 mm rough platelets (*Rough*); the second sample is an ooid sand with smooth and round grains having a lustrous surface, with diameters between 0.25 and 0.5 mm (*Sample A*). Both of these samples were collected near Lee Stocking Island, Bahamas. The third sediment is a volcanic beach sand (*Volcanic*) with diameters between 0.25–0.5 mm and a very low plane albedo (approximately 0.02) collected from Big Island, Hawaii. The spheres (*Spheres*) used are nearly mono-disperse polymer spheres with a nominal diameter of 0.2 mm (Duke Scientific 4320A) [18]. This collection of samples is representative in that it covers a range of optical characteristics: from darkest *Volcanic* to nearly non-absorbing *Spheres* (estimated single scattering albedo = 0.999 [18]). In previous measurements the *Rough* sample had the strongest hotspot, but no forward scattering lobe while *Sample A* had both a hotspot and forward peak [21].

#### *Rough*

Figure 2 displays the REFF, DOP and  $\mu_c$  of sample *Rough* at normal and 60°-illumination. At normal illumination the REFF shows a slight gradual increase towards small phase angle then a narrow increase right around 0° phase angle, which is often seen in sediment REFF's [20,21]. At 60° incident angle the REFF shows a very strong backscattering peak with no evidence of an increase in the forward direction and a very small bump in the specular direction (around 120° phase angle). For both the normal illumination and 60° illumination the DOP (Fig. 2(b)) clearly shows a small BNP feature below 25° phase angle, reaching a minimum about -2% around 5° phase angle. The  $\mu_c$  curve (Fig. 2(c)) shows a decrease from larger phase angles but no prominent increase towards 0° phase angle near the opposition. The DOP and  $\mu_c$  parameters are noisy. As mentioned in Section 2, this is caused by (1) the polarization measurements yielding a lower S/N ratio and (2) the large grain size of this sample introducing more measurement uncertainties because of the influence of the large facets. However, both the BNP of the DOP curves and the  $\mu_c$  trend were reliably reproduced in repeated measurements on different surface realizations of this sample. Note that in this sample,  $\mu_c$  at opposition is approximately 0.90 indicating that 6% of the incident circularly polarized light is still circularly polarized, although with opposite helicity.

#### *Sample A*

Figure 3 shows the results for *Sample A*. As pointed out in our earlier work [21], this sample displays indications of a forward scattering peak (3(a)) at oblique incident angles. The DOP and  $\mu_c$  seem to be totally structureless for phase angles <60°. At phase angles >60° the DOP increases slightly towards larger phase angles (Fig. 3(c)). At phase angles >100° (forward scattering) both DOP and  $\mu_c$  increase strongly. This region is where the REFF is also increasing strongly. Also note that  $\mu_c$  approaches 0.97 in this sample indicating that only 2% of the incident circularly polarized light is still circularly polarized.

#### *Volcanic*

Figure 4 shows the results for *Volcanic*. One might conjecture that such a low albedo surface would have the single particle phase function manifested in a reflectance measurement.

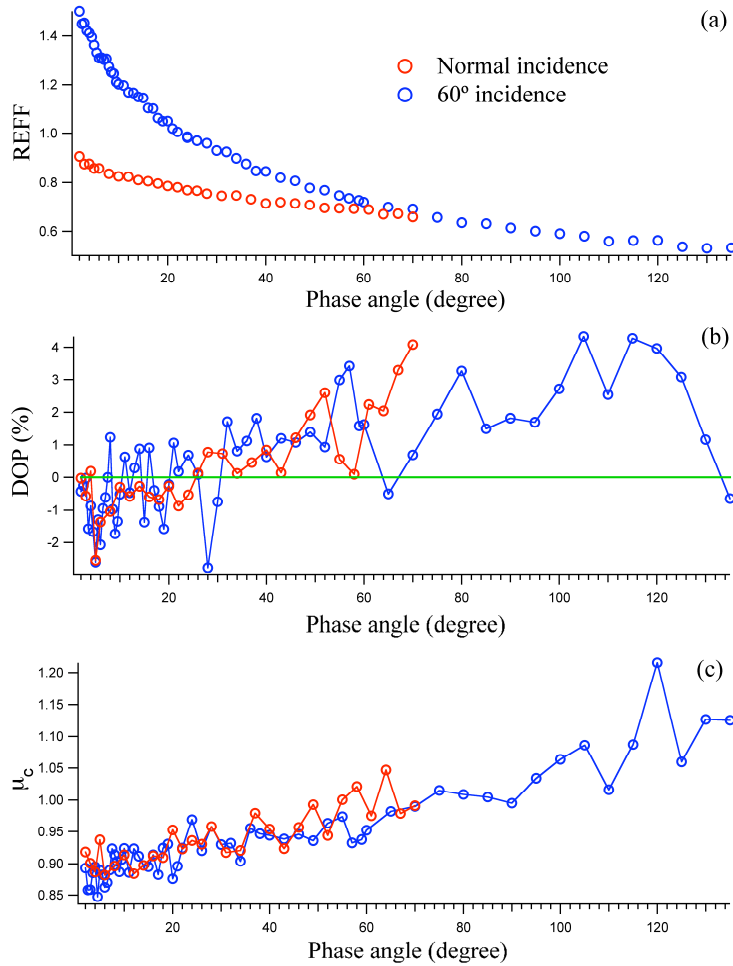


Fig. 2. (a) REFF (b) degree of polarization (DOP) and (c)  $\mu_c$  of sample *Rough* at normal and 60° illuminations. To aid the identification of the BNP, DOP=0 is shown as the green line in (b).

However, comparison of normal and 60° shows that considerable differences exist in the two scattering configurations, meaning multiple scattering still plays a role in the reflectance. The DOP and  $\mu_c$  decrease consistently from large phase angles and no BNP or increased  $\mu_c$  can be found.

Compared with the previous two benthic sediments, two prominent features can be found for *Volcanic* besides the much lower REFF values: (1) the much higher DOP values in several tens of percent in contrast to several percent for the other samples at large phase angles and (2) the much lower  $\mu_c$  values at small phase angles. This is explained by the Umov effect [1] that states that high albedo objects tend to reflect mostly unpolarized light and low albedo objects tend to reflect polarized light. Once again note that while this sample also has DOP = 0 at 0° phase angle, as would be expected due to symmetry,  $\mu_c$  is much lower (approximately 0.5). Thus 34% of the light maintains its circular polarization.

#### Linear Polarization Ratio

Although no CBS feature could be detected in measurements on sediments, an interesting aspect of these results is the application to various techniques that use polarization for

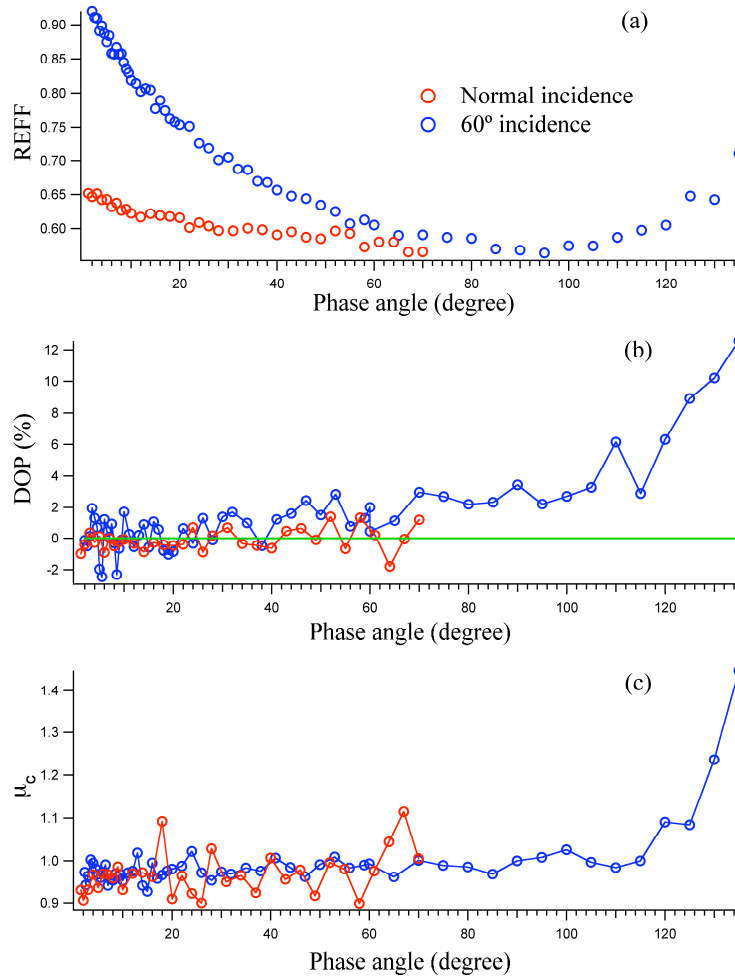


Fig. 3. Same as Fig. 2 but for *Sample A*.

discrimination between target vs. medium backscattered light [15-17]. The natural samples we measured had varying  $\mu_c$  near opposition. The smooth *Sample A* almost completely depolarizes the incident circularly polarized light. Thus circular polarization will be an effective discrimination technique between backscattered light from the sediment target and intervening media. *Sample Rough* depolarizes 94% of the incident light, while the volcanic sample only depolarizes 66% of the incident light.

To see if the two benthic sediments *Rough* and *Sample A* have a similar depolarizing behavior under linearly polarized illumination, we measured  $\mu_{\perp}$  and  $\mu_{\parallel}$  at  $8^{\circ}$  illumination. We chose this incidence angle because the polarization characteristics of the sediments are quite insensitive to incident zenith angles as shown in Figs. 2-4, and the  $8^{\circ}$ -incidence has a higher SNR than  $60^{\circ}$  incidence. Figure 5 and Fig. 6 display  $\mu_{\perp}$  and  $\mu_{\parallel}$  at  $8^{\circ}$ -incidence for *Rough* and *Sample A*, respectively. These results demonstrate that near the backscattering direction *Rough* and *Sample A* depolarize 89% and 95% of the incident linearly polarized light, respectively.



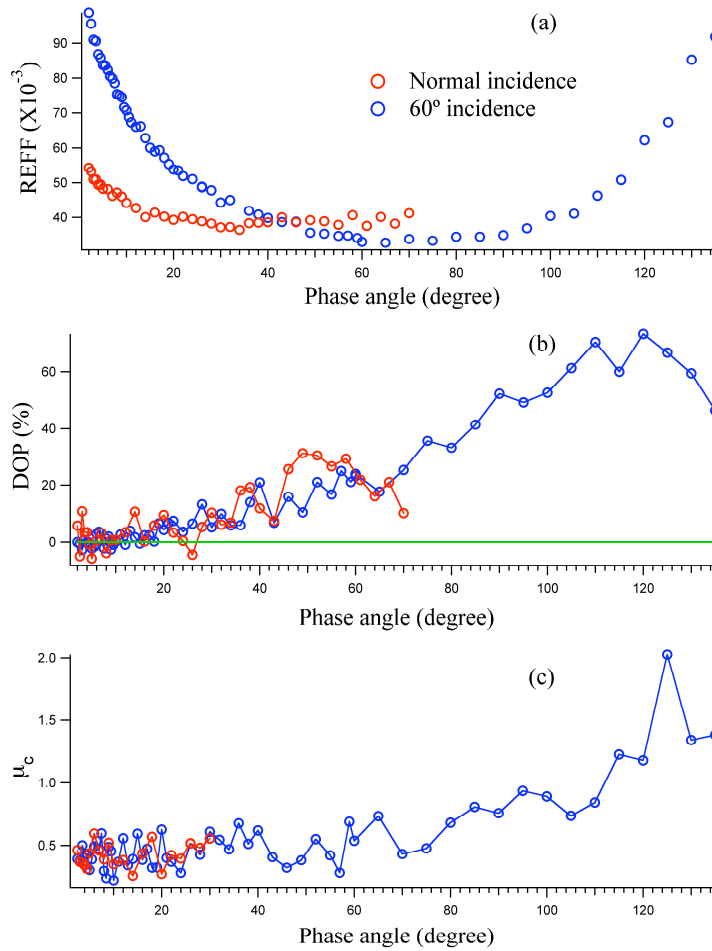


Fig. 4. Same as Fig. 2 but for *Volcanic*.

### Spheres

Figure 7 shows the results for *Spheres*. Because of the nearly perfect spherical shape this sample has much richer angular structure than the sediments introduced earlier. Even with an optically thick layer (optical thickness of 87.5) and single scattering albedo of 0.999 for individual grains [18], scattering features around the primary ( $15^\circ$  phase angle) and second order rainbows (the much weaker peak around  $102^\circ$  phase angle, shown in  $60^\circ$ -incidence) are retained.

As the computation of the reflectance of polarized light from closely packed media especially those composed of very large grains, is still a challenge, here we plot a comparison of the measurements with Mie single scattering calculations [26] in an attempt to identify the remnant single scattering features.

It is well-known that spheres have a Mueller matrix of the form [27]

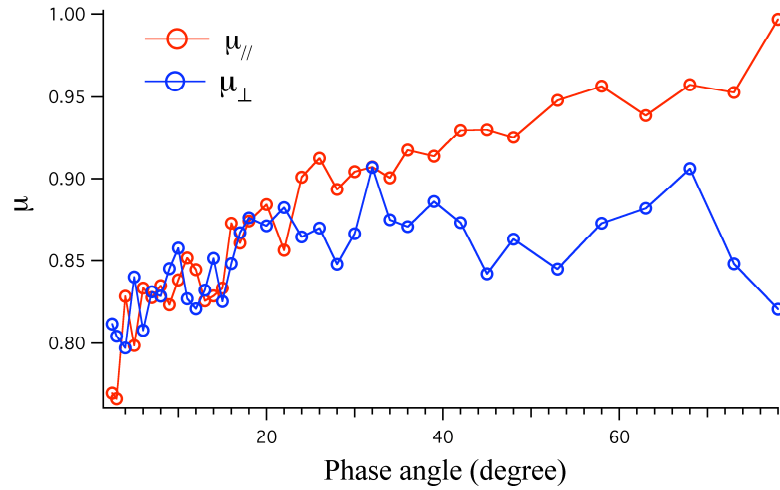


Fig. 5. Linear polarization ratios  $\mu_{\perp}$  and  $\mu_{\parallel}$  of sample *Rough* at  $8^{\circ}$  illumination.

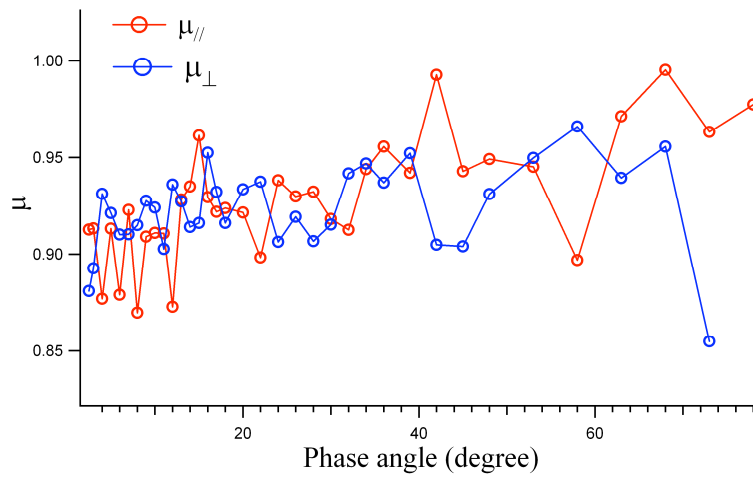


Fig. 6. Linear polarization ratios  $\mu_{\perp}$  and  $\mu_{\parallel}$  of *Sample A* at  $8^{\circ}$  illumination.

$$M_{ij} = \begin{bmatrix} M_{11} & M_{12} & 0 & 0 \\ M_{12} & M_{11} & 0 & 0 \\ 0 & 0 & M_{33} & M_{34} \\ 0 & 0 & -M_{34} & M_{33} \end{bmatrix}. \quad (4)$$

For DOP, the incident light is randomly polarized and  $DOP = -\frac{M_{12}}{M_{11}}$  while

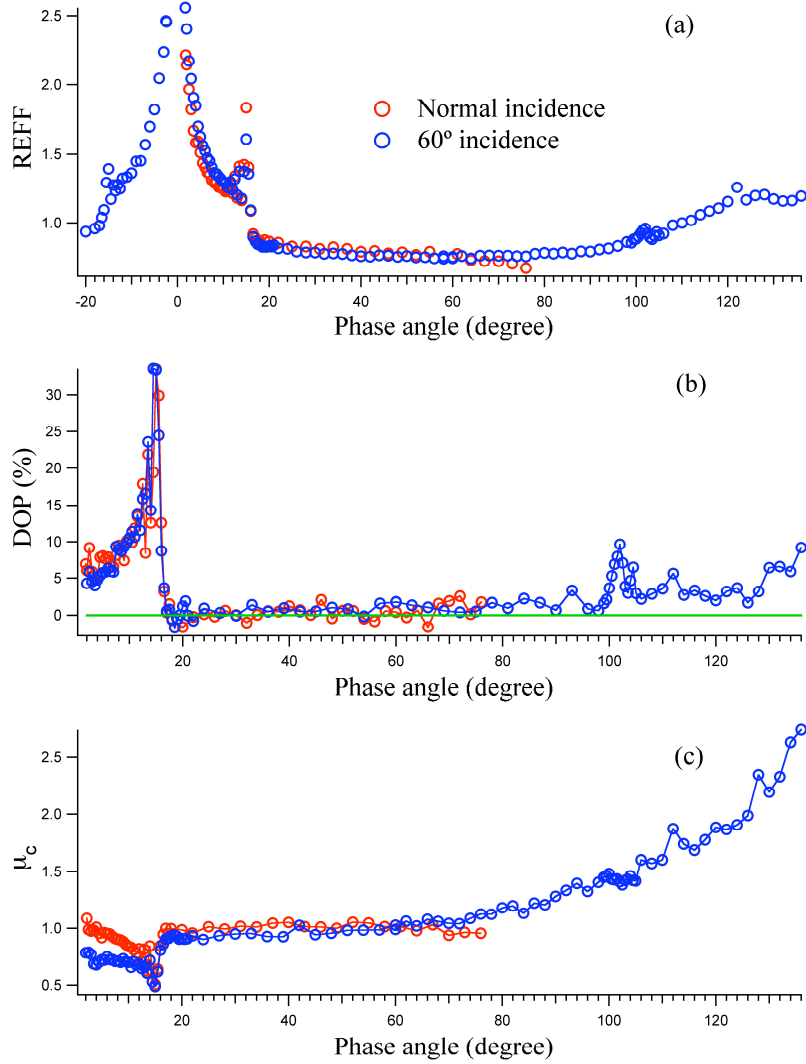


Fig. 7. Same as Fig. 2 but for Spheres. Negative phase angle stands for  $180^\circ$  relative azimuth angle between incident and viewing directions. Note the denser data points around the rainbows around  $15^\circ$  and  $102^\circ$ , see Figs. 8-9 for more detailed angular structures.

$$\mu_c = \frac{M_{11} + M_{33}}{M_{11} - M_{33}} \quad (5)$$

and  $\mu_L = 0$ .

Figure 8 shows comparisons of a packed layer measurement result and Mie computations. For comparison purposes we convert the Mie phase function  $P(g)$  to reflectance factor (REFF) using

$$REFF = \frac{\varpi_0}{4(\mu_0 + \mu)} P(g). \quad (6)$$

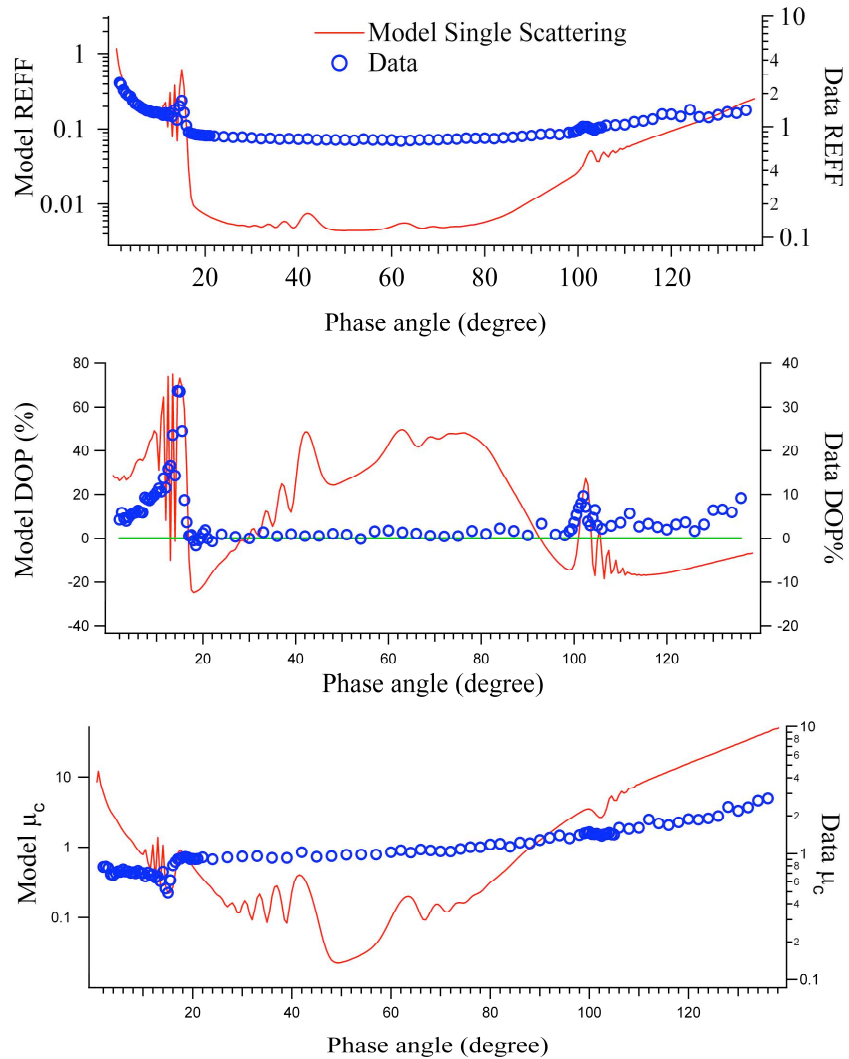


Fig. 8. Comparisons of gonio measurement at  $60^\circ$  illumination and single scattering calculations for *Spheres*: REFF (top), DOP (middle) and circular polarization ratio  $\mu_c$  (bottom).

The comparisons between gonio and Mie results for REFF, DOP and  $\mu_c$  at  $60^\circ$  incidence seem quite consistent with each other. Near both the first ( $15^\circ$ ) and second ( $102^\circ$ ) order rainbows the surface retains the major single scattering features; but the single scattering features in between are washed out. This is because the single scattering component is about 50% (near the first order rainbow) and 10% (near the second order rainbow) of the total intensity while only  $<3\%$  in the regions between, as demonstrated by the REFF. This explains why many subtle angular structures of single scattering are preserved around these regions. For example, the DOP curve for the packed layer shows a DOP value of +34% over the first order rainbow peak but drops down to -1.6% just above the rainbow peak (around  $18^\circ$  phase angle), which is clearly a remnant of the single scattering feature (first order rainbow is strongly positively polarized but just above the peak the DOP drops to -20%). Similarly, the  $\mu_c$  curve for the packed layer has features of single scattering but is much flatter. A comparison of  $\mu_c$  at normal and  $60^\circ$  incidences (Fig. 7(c)) shows that the increase is stronger

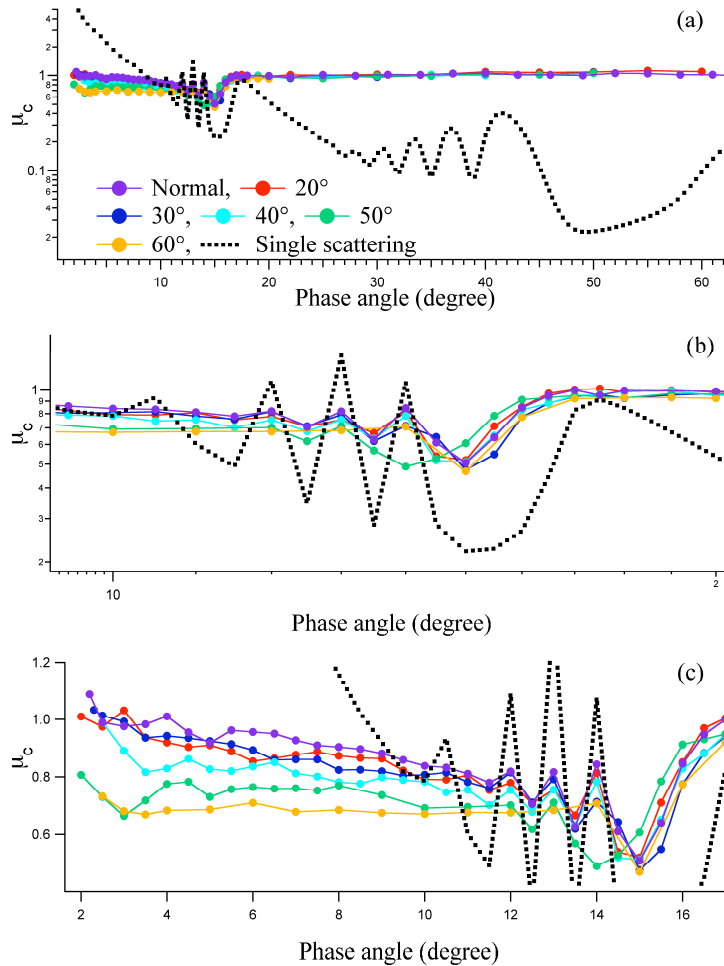


Fig. 9. Measured *Spheres*  $\mu_c$  at incident angles at normal, 20°, 30°, 40°, 50° and 60°, with calculated  $\mu_c$  for single scattering, (a) overall comparison (b) comparisons near the first order rainbow and (c) measured  $\mu_c$  near the opposition.

for normal illumination than for 60°. To investigate this further we measured  $\mu_c$  at 20°, 30°, 40° and 50° illumination angles for phase angle  $<60^\circ$  and the results are shown in Fig. 9. Figure 9(a) shows that the  $\mu_c$  values above the 1<sup>st</sup> order rainbow peak are equal but diverge below the rainbow. Figure 9(b) shows that the major single scattering peaks at 12°, 13° and 14° are clearly preserved for packed  $\mu_c$  (except for 50° incidence's 14° peak). Under these five illumination angles  $\mu_c$  indeed climbs higher toward opposition, and the general trend in progression of decreasing  $\mu_c$  from normal to 60° illumination is seen in Fig. 9(c), though not clearly at the minimum phase angle 2°. Even with such an increased  $\mu_c$  toward opposition, it is very likely this is a single scattering feature instead of the CBS feature, as Fig. 8 shows the single scatter  $\mu_c$  increases strongly at small phase angles. Thus the strong backscattering feature observed in reflectance measurements should mainly come from single particle scattering. It should be noted that  $\mu_c$  is zero at zero phase angle for spheres, but it increases sharply to non-trivial values once phase angle is away from exact zero.

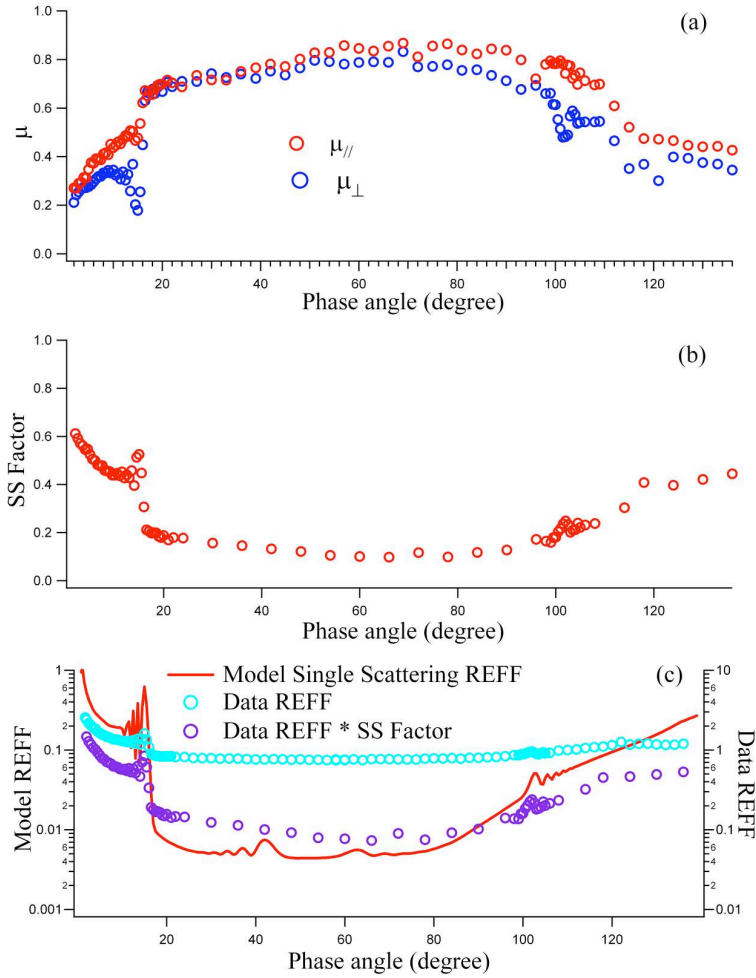


Fig. 10 (a) Linear polarization ratios  $\mu_{\perp}$  and  $\mu_{\parallel}$ , (b) single scattering factor (SS Factor) and (c) comparisons of measured REFF (Data REFF), the SS Factor corrected REFF (Data REFF\*SS Factor) and single scattering REFF (Eq.(6)) under  $60^{\circ}$  illumination.

Figure 10 displays (a) the linear polarization ratios  $\mu_{\perp}$  and  $\mu_{\parallel}$ , (b) the polarization scaling factor, and (c) both the measured and scaled REFF, all at  $60^{\circ}$  illumination. As spheres should have a zero value for both  $\mu_{\perp}$  and  $\mu_{\parallel}$  under single scattering condition, the non-zero values of  $\mu_{\perp}$  and  $\mu_{\parallel}$  may provide us a first order method to discriminate single scattering from multiple scattering. Given the definition of  $\mu_{\parallel}$ , The fraction polarized reflected light, for incident polarized light, is:

$$Fraction_{\perp} = \frac{I_{PP} - I_{PS}}{I_{PP} + I_{PS}} = \frac{1 - \mu_{\parallel}}{1 + \mu_{\parallel}} \quad (7)$$

Similarly one can form this fraction for incident parallel polarized light. Assuming that this is, to first order, the fraction of single scattering light to total reflected light, one can average these numbers for perpendicular and reflected and obtain what we are calling the SS Factor in Fig 10(b). Being consistent with the results presented in Fig. 8, the  $\mu_{\perp}$  and  $\mu_{\parallel}$  curves shown

in Fig. 10(a) demonstrate that strongest multiple scattering occurs between the first and second order rainbows, as evidenced by their deviations from zero. Figure 10(c) is the application of this factor to the measured REFF (unpolarized incidence), and the comparison of this with that predicted by Eq. 6. Figure 10(c) shows that, even after multiplying the SS Factor shown in Fig. 10(b), the single scattering REFF still could not be recovered from REFF of a packed layer. It is not surprising because part of the multiple scattered light will probably remain partially polarized.

#### 4. Conclusions

For rough sediment a branch of negative polarization was detected below  $25^\circ$  phase angle while for smooth grains no negative polarization was found. This could be used in shallow water remote sensing to distinguish sediments with smooth and rough surfaces. Currently sample *Rough* is the only benthic sediment in our collection that has a rough grain surface. If more large and rough benthic sediments were measured, looking for the branch of negative polarization may be used to distinguish between rough and smooth particles. However even in this case, the degree of polarization of negative polarization was very small (less than 2%). For circular polarization, no apparent increase towards zero phase angle could be found and thus no strong evidence of the CBS in sediments. For spheres, several single scattering features are retained in this strongly multiple scattering medium. Comparisons of single scattering features of individual spherical particles and packed layer show that the strong backscattering and negative polarization come from single particle features.

The circular polarization ratio and linear polarization ratio measurements show that the smooth ooids (*Sample A*) is a nearly perfect circular depolarizer and an effective linear depolarizer (~95%), while the rough platelets (*Rough*) depolarize 94% of the circular incidence and 90% of the linear incidence, thus is also a strong depolarizer. In contrast, the Umov effect makes the nearly totally absorbing *Volcanic* quite polarizing, making circular polarization discrimination techniques less effective. The DOP measurements indicate that the backscattered light will be almost linearly unpolarized from sediments, when the incident light is also unpolarized. However in this case both pure water and particulate media will not linearly polarize light in the backscattering direction, hence linear polarization will not be an effective technique for target (sediment) discrimination.

#### Acknowledgment

We are indebted to the late Albert Chapin for help in instrumentation and measurement. We also thank the constructive comments and some clarifications by the anonymous reviewers. This work was supported by the Office of Naval Research Ocean Optics Program.